Electronic Supplementary Information (ESI)

Multifunctional NiO/Ti^{3+}-TiO_2 for concurrent Water Reduction and Glycerol Oxidation to Value added products by Sunlight driven photocatalysis

Sivaraj Rajendran, [a] Simi Saju, [a] Sunesh S. Mani, [a] Anantha Krishnan Asoka, [a] Arindam Saha,[b,c] Pushkaran S. Arun, [a] Biplab Ghosh, [d] Thomas Mathew, [a,*] and Chinnakonda S. Gopinath [b,c,*]

[a] Department of Chemistry, St. John's College (Affil. University of Kerala), Anchal, Kerala – 691306, India, E-Mail: thomasmathew@stjohns.ac.in
[b] Catalysis and Inorganic Chemistry Division, CSIR - National Chemical Laboratory, Dr. Homi Bhabha Road, Pune 411 008, India. E-mail: cs.gopinath@ncl.res.in.
[c] Academy of Scientific and Innovative Research (AcSIR), Ghaziabad 201002, India
[d] Beamline Development & Application Section, Bhabha Atomic Research Center, Mumbai 400085, India.

Supplementary Text:

The spectra of all the catalyst materials were recorded in grazing in fluorescence mode while that of references (Ni foil and NiO) in transmission mode. In fluorescence mode, the sample is kept at 45° to the incident X-ray beam and a silicon drift detector kept in the horizontal plane at 90° to the incident X-ray beam were employed to measure the incident flux (I_0) and florescence signal (I_f) from the sample. Then the absorption coefficient (μ) is obtained by using the relation $\mu = \frac{I_f}{I_0}$

In transmission mode, three ionization chambers were used for measuring incident flux (I_0), transmitted flux (I_t) and the XAS spectrum of a reference metal foil for calibration. The absorption coefficient (μ) was obtained using the relation, $I_t = I_0 e^{-\mu x}$, where x is the thickness of the material. The beamline uses a double crystal monochromator (DCM) with an operating energy range of 4-25 keV. Data processing and analysis were carried out using different data analysis programs available in the Demeter software package. The Athena module was employed for background removal, pre-edge and post-edge corrections, normalization, Fourier transform, etc. Finally, the Artemis module was employed for fitting the experimental data (raw data) against the scattering paths generated from crystallographic $NiTiO_3$ data using the FEFF 6.0 code. The fitting widow used for all fits is 1 to 3.4 Å, and we have also included background in the final fit.

Table S1. XPS parameters and porous characteristics obtained from N_2 adsorption-desorption analysis of TiO_2 and NiO/Ti^{3+}-TiO_2 (NiT) photocatalysts. [a](SOC) indicates spin–orbit coupling separation.

Photocatalyst	BE of O1s [eV]	BE of Ni $2p_{3/2}$ [a](SOC)[eV]	BE of Ti $2p_{3/2}$ [a](SOC) [eV]	KE of Ni LMM [eV]	Auger parameter (α')	S_{BET} [m^2g^{-1}]	Pore size [nm]	V_p [mLg^{-1}]
TiO_2	529.4, 530.36 and 532	NA	458.5 (5.9)	NA	NA	22.1	4.9	0.050
NiT-1	528.2,529.65 and 530.35	855.50(17.8)	457.40, 458.4 (5.8,5.7)	843.25	1698.7	24.1	5.6	0.052
NiT-2	528.2,529.6 and 530.4	855.45(17.8)	457.20,458.34 (5.9,5.8)	843.52	1698.9	NA	NA	NA
NiT-3	528.2,529.6 and 530.45	855.40(18.1)	457.05,458.38 (5.9,5.7)	843.65	1699	27.1	4.3	0.065
NiT-4	528.1., 529.7 and 530.7	855.30(17.8)	457.07,458.42 (5.9,5.8)	843.95	1699.2	NA	NA	NA

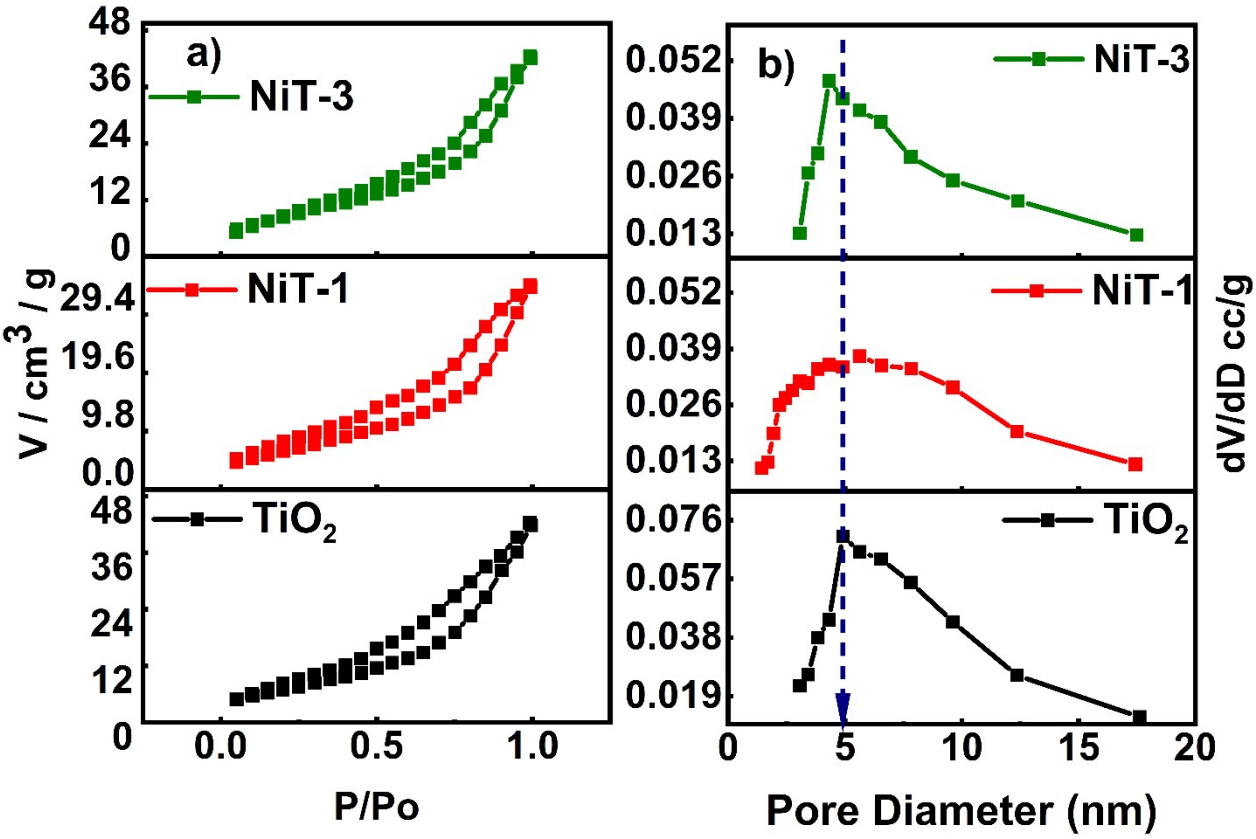

Figure S1. (a) N_2 adsorption-desorption isotherms, and (b) pore size distribution pattern of TiO_2, and representative samples. Pore size distribution was estimated by the BJH model from N_2 adsorption–desorption isotherm.

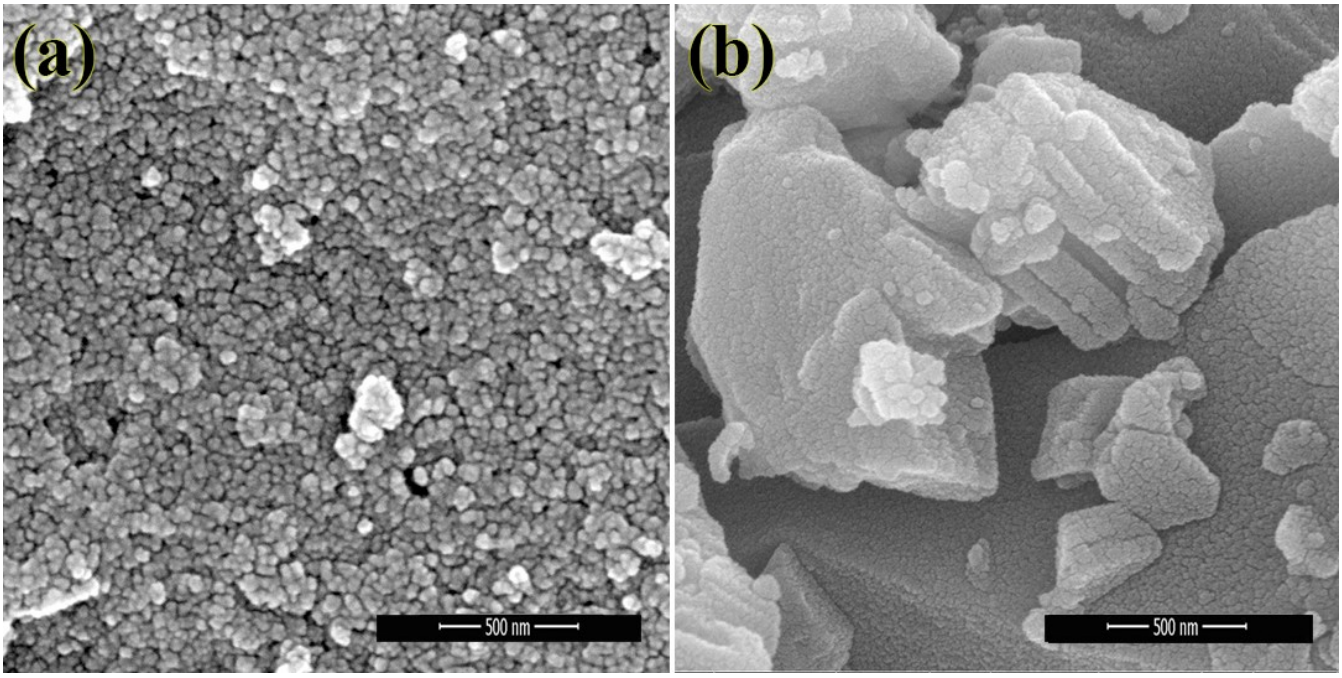

Figure S2. FESEM images of TiO_2 and NiO/Ti^{3+}-TiO_2 nanocomposites: (a) TiO_2 and (b) NiT-3.

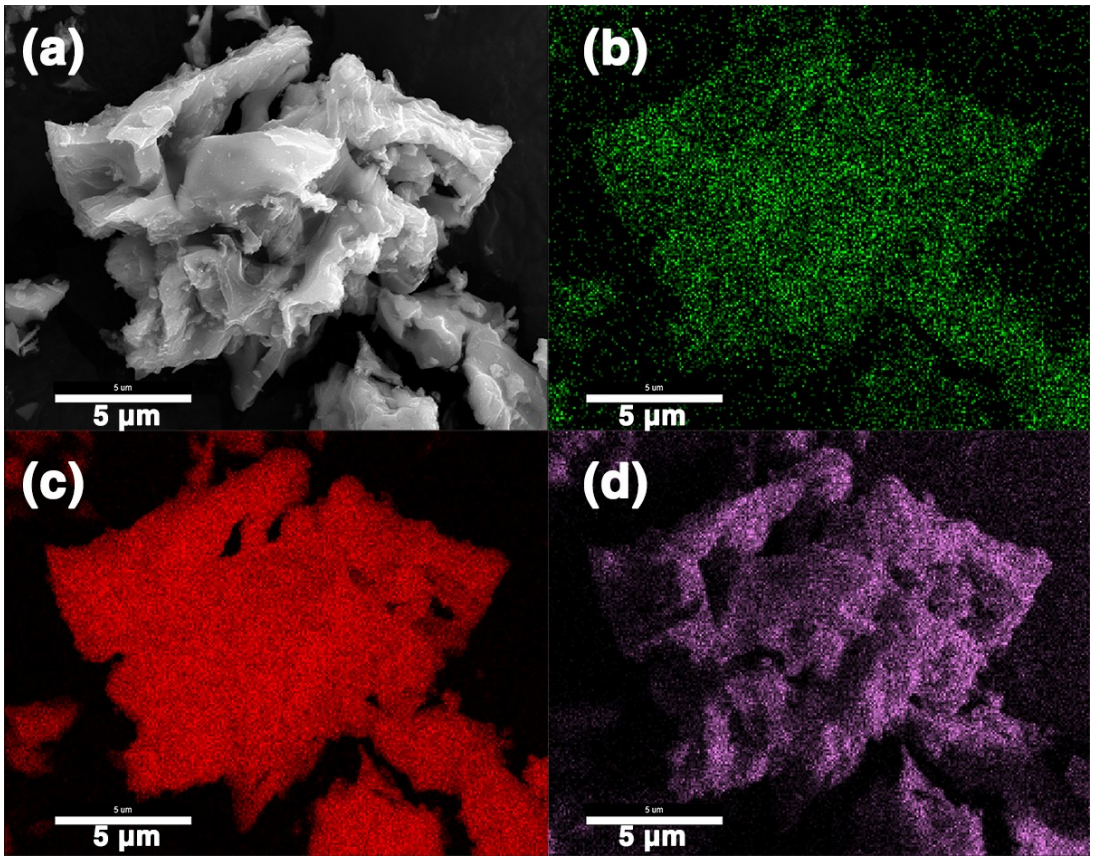

Figure S3. The EDS mapping of NiT-3: (a) FESEM, (b) Ni, (c) Ti, and (d) O, reveals uniform dispersion of Ni on the surface of TiO_2.

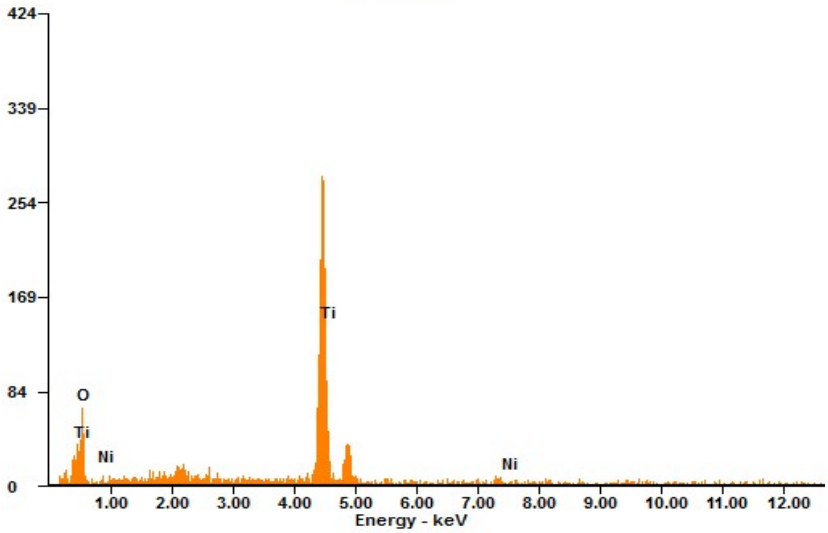

NiO/Ti^{3+}-TiO_2	Ti %	Ni %
NiT-1	98.8	1.18
NiT-2	97.6	2.39
NiT-3	96.4	3.6
NiT-4	95.3	4.69

Figure S4. The energy dispersive X-ray analysis (EDX) was employed to confirm the elemental composition of all composites and the results for NiT-3 is shown**.** Table shows the atom percent of Ti and Ni in NiO/Ti^{3+}-TiO_2 nanocomposites.

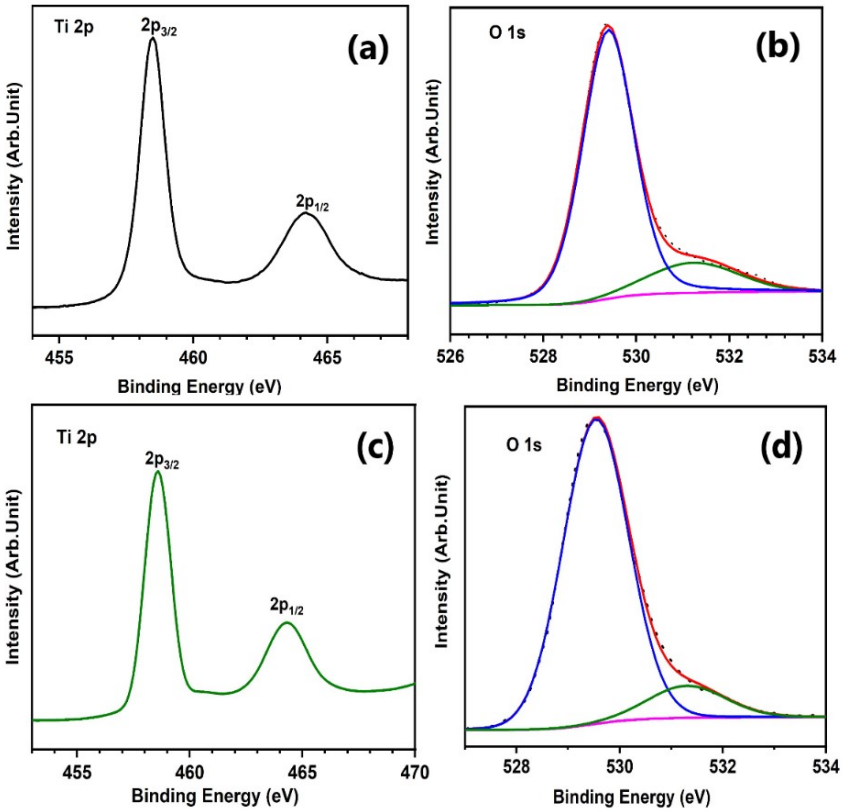

Figure S5. XPS spectra recorded for Ti 2p, and O 1s core level from TiO_2 (a and b) and NiO/TiO_2 composite catalyst prepared by conventional impregnation method (c and d).

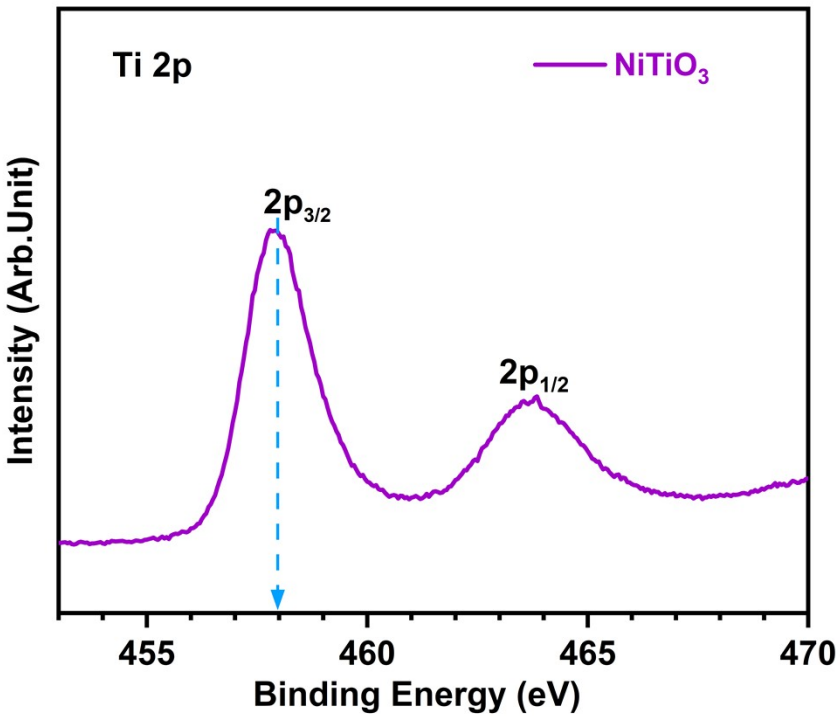

Figure S6. XPS spectra for Ti 2p core levels for $NiTiO_3$.

Table S2. Ni K-Edge Positions obtained for Ni foil, NiO standard and NiT nanocomposites

Sample	Edge position (eV)
Ni metal	8333.1
NiO	8345.5
NiT-1	8345.0
NiT-2	8345.1
NiT-3	8344.6
NiT-4	8344.4

Table S3. Structural parameters obtained from the Ni K-edge EXAFS fittings (coordination number (N), interatomic distance (R), Debye–Waller (σ^2), edge-energy correlation (ΔE).

NiO						
	N	S_0^2	**ΔE_0**	**R (Å)**	σ^2**(Å²)**	**R-factor**
[NiO] O1.1	6	1	-4.0271	2.06±0.09	0.006±0.001	0.008
[NiO] Ni1.1	12	1	-4.0271	2.95±0.05	0.007±0.0003	
NiT-1						
[$TiNiO_3$] O2.2	3.6 ±0.6	0.608 ±0.112	-3.796	1.99±0.08	0.001±0.002	0.030
[$TiNiO_3$] Ti0.1	0.6 ±0.1	0.608 ±0.112	-3.796	2.74±0.07	0.001	
[$TiNiO_3$] Ni1.1	1.8±0.3	0.608 ±0.112	-3.796	2.89±0.04	0.003	
[$TiNiO_3$] O2.3	1.8±0.3	0.608 ±0.112	-3.796	3.72±0.34	0.003	
[$TiNiO_3$] Ti0.2	1.8±0.3	0.608 ±0.112	-3.796	3.59±0.20	0.003	

NiT-2						
[$TiNiO_3$] O2.2	4.1 ±0.2	0.692 ±0.039	2.514	2.06±0.01	0.001	0.004
[$TiNiO_3$] Ti0.1	0.6 ±0.03	0.692 ±0.039	2.514	2.39±0.42	0.006±0.001	
[$TiNiO_3$] Ni1.1	2.0±0.1	0.692 ±0.039	2.514	2.94±0.04	0.001	
[$TiNiO_3$] O2.3	2.0±0.1	0.692 ±0.039	2.514	3.71±0.33	0.001	
[$TiNiO_3$] Ti0.2	2.0±0.1	0.692 ±0.039	2.514	3.39±0.01	0.009±0.002	
NiT-3						
[$TiNiO_3$] O2.2	5.7	0.95	0.590	2.07±0.01	0.009±0.001	0.005
[$TiNiO_3$] Ti0.1	0.95	0.95	0.590	3.16±0.34	0.001	
[$TiNiO_3$] Ni1.1	2.85	0.95	0.590	2.90±0.03	0.002±0.001	
[$TiNiO_3$] O2.3	2.85	0.95	0.590	3.60±0.22	0.003	
NiT-4						
[$TiNiO_3$] O2.2	5.0±0.9	0.841±0.152	4.041	2.04±0.04	0.005±0.003	0.029
[$TiNiO_3$] Ti0.1	0.8±0.1	0.841±0.152	4.041	2.83±0.01	0.001	
[$TiNiO_3$] Ni1.1	2.5±0.4	0.841±0.152	4.041	2.92±0.03	0.001	
[$TiNiO_3$] O2.3	2.5±0.4	0.841±0.152	4.041	3.60±0.22	0.003	
[$TiNiO_3$] Ti0.2	2.5±0.4	0.841±0.152	4.041	3.36±0.02	0.004	

Figure S7. UV-Vis absorption spectra (a) and band gap (b) of pure NiO.

Table S4. The decay lifetimes and the average lifetime of photoexcited charge carriers in TiO_2 and NiT-3 calculated using tri-exponential decay equation.

Parameters	Samples	
	TiO_2	**NiT-3**
τ_1 (ns)	0.48	1.49
τ_2 (ns)	0.96	1.26
τ_3 (ns)	1.94	7.59
τ_{avg} (ns)	1.85	6.69
χ^2 (goodness of fitting)	0.99	0.99

The average lifetime (τ_{avg}) can be estimated using the following equation **S1**:

$$\tau_{avg} = \frac{A_1\tau_1^2 + A_2\tau_2^2 + A_3\tau_3^2}{A_1\tau_1 + A_2\tau_2 + A_3\tau_3}$$

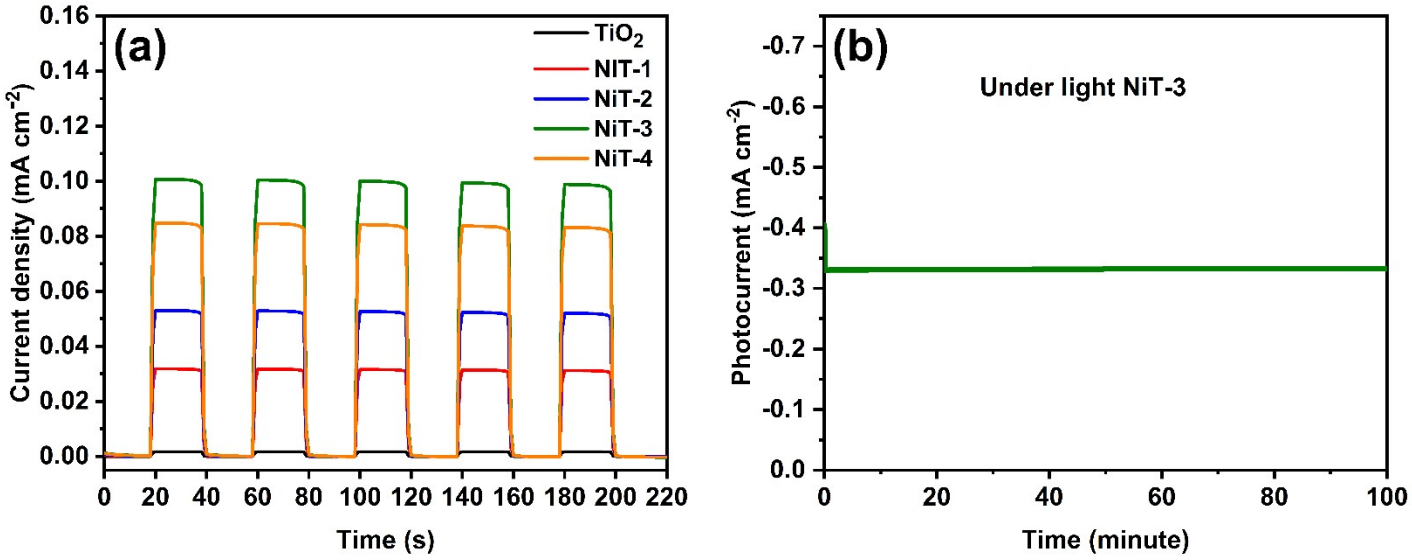

Figure S8. (a) Transient photocurrent density profiles of TiO_2 and NiT photoelectrodes in 0.1M glycerol + 1M KOH. (b) Photostability test for NiT-3 photoelectrode under continuous light illumination in 1M KOH.

Table S5. Fitting values of EIS parameters obtained for TiO_2 and NiT photoelectrodes.

Parameters	**TiO_2**	**NiT-1**	**NiT-2**	**NiT-3**	**NiT-4**
Solution Resistance (Rs)/Ω	0.80	0.72	0.66	0.58	0.60
Double Layer Capacitance (C_{dl})/μF	51.81	91.23	134.56	451.95	181.44
Charge Transfer Resistance (R_{ct})/Ω	2010.86	1282.78	1080.15	270.90	743.55

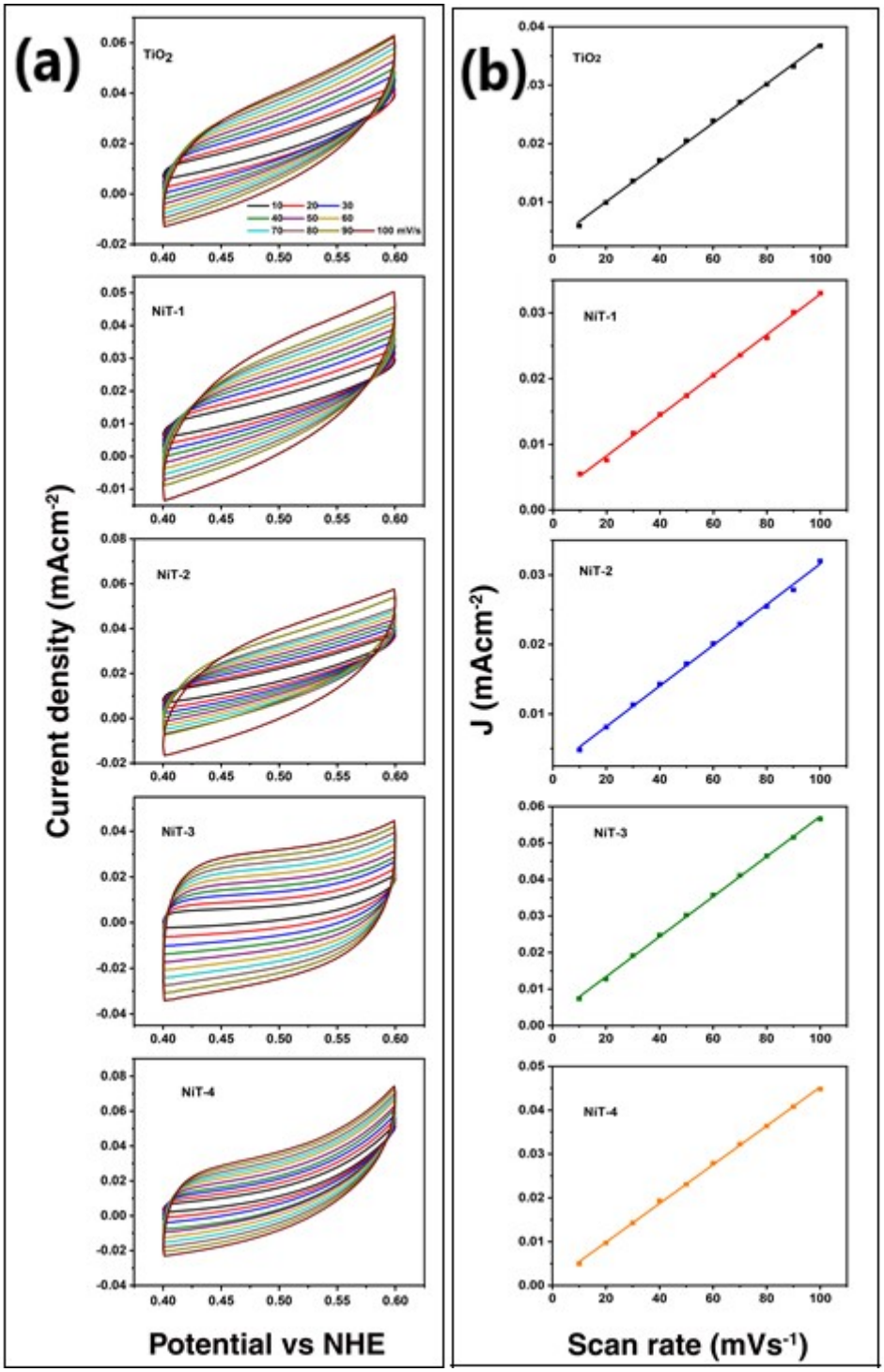

Figure S9. The Electrochemical capacitance measurements to determine the electrochemically active surface area (ECSA) of the catalysts in 1 M KOH. (a) The capacitive current density on TiO_2 and NiT nanocomposites from double layer charging can be obtained from cyclic voltammograms (CV) at different scan rates in the non-Faradic region. (b) The measured capacitive current (j) was plotted as a function of scan rate to calculate double layer capacitance (C_{dl}).

Calculations of ECSA for TiO_2 and NiT nanocomposites

Double layer capacitance (C_{dl}) was obtained by estimating half the value of slope between Δj at different Scan rates of 10 to 100 mVs^{-1} in a non-Faradaic region between 0 .4 and 0.6 V vs NHE.
For example, in the case of NiT-3, C_{dl}= 0.2808 mF

Cs = 0.040 $mFcm^{-2}$ at 1M KOH[1]
Where Δj is change in capacitive current at different scan rates and Cs is specific capacitance.

ECSA= C_{dl}/Cs = 0.2808/0.040

= 7.02 cm^2

Table S6. Calculated C_{dl} and ECSA values TiO_2 and NiT nanocomposites as obtained from **Figure S9**.

Sl. No	Catalyst	C_{dl} ($mFcm^{-2}$)	ECSA (cm^2)
1	TiO_2	0.1202	3.0
2	NiT-1	0.1538	3.85
3	NiT-2	0.1685	4.21
4	NiT-3	0.2808	7.02
5	NiT-4	0.2214	5.53

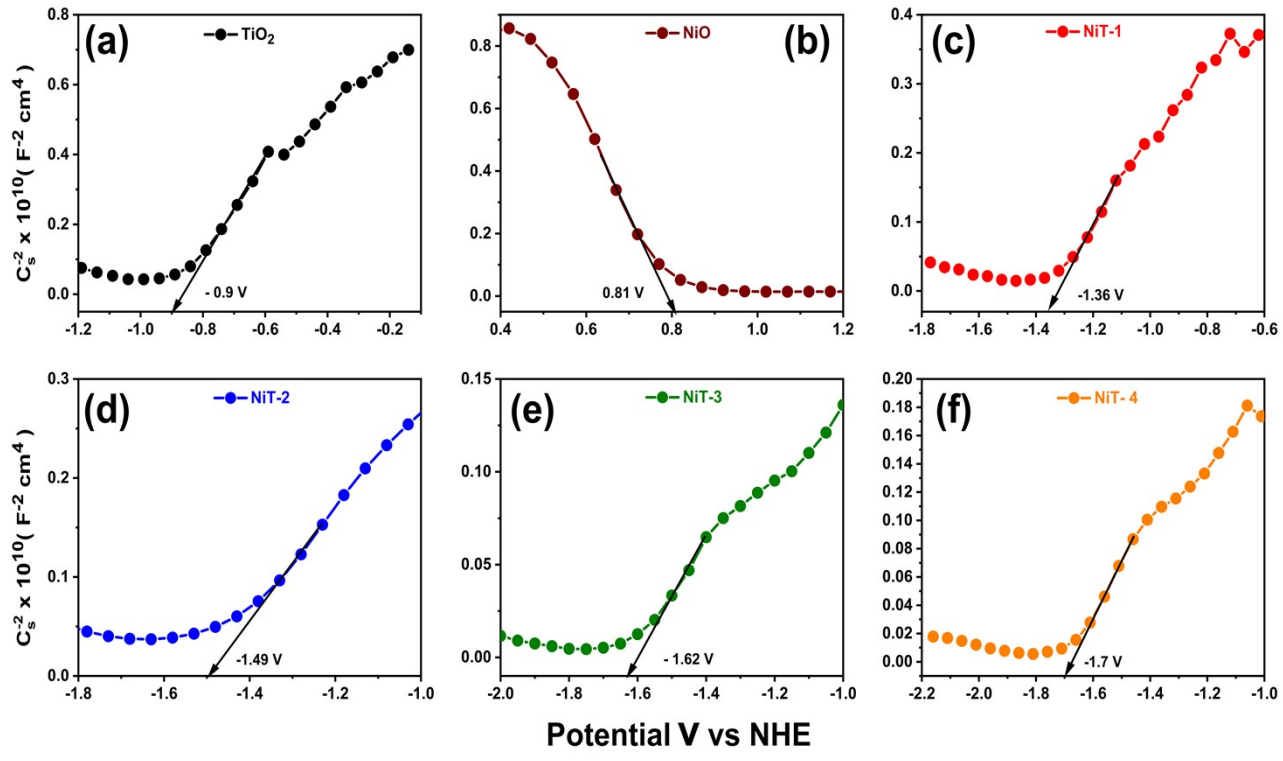

Figure S10. Mott−Schottky plots of TiO_2, NiO and NiT nanocomposites.

The donor concentration of TiO_2 and NiT nanocomposites were calculated using MS equation (**S2**).[2]

$$\frac{1}{C_S^2} = \frac{2}{q\varepsilon_r\varepsilon_0 N_D}(V_{ap} - V_{fb} - \frac{k_B T}{q}) \quad \text{(S2)}$$

Where N_D, q, ε_r, ε_o, V_{ap}, V_{fb}, and ^{k_B}T are the donor concentration/ the charge carrier density, electronic charge, the relative permittivity of semiconductor, permittivity of vacuum, applied potential, flat band potential and Boltzmann energy term, respectively. The ^{k_B}T term was negligible compared to other parameters and it was assumed that the values of q, ε_r and ε_o are same for both TiO_2 and NiT nanocomposites.

Table S7. The apparent quantum yield (AQY) of TiO_2 and NiT nanocomposites calculated at different wavelengths (nm).

Wavelength (nm)	**AQY % of TiO_2**	**AQY % of NiT-1**	**AQY % of NiT-2**	**AQY % of NiT-3**	**AQY % of NiT-4**
410	0.12	1.03	1.62	4.28	3.25
490	0.01	0.65	1.05	2.26	1.53

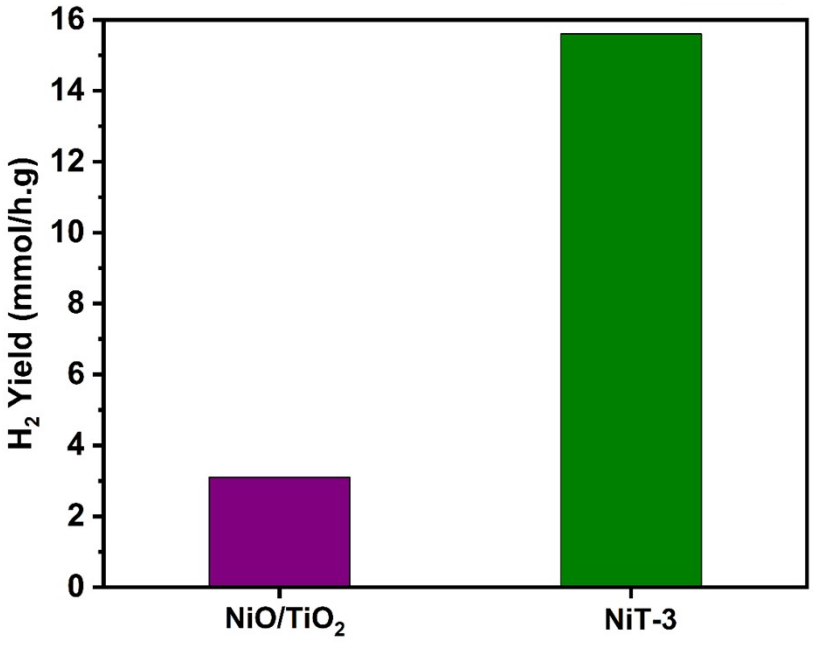

Figure S11. Comparison of photocatalytic H_2 production efficiency of thin film form of NiT-3 and NiO/TiO_2 prepared by traditional impregnation method with same Ni /Ti ratio as that of NiT-3. A five-fold higher H_2 production rate was obtained with NiT-3 compared to the catalyst prepared by the traditional method, which does not contain Ti^{3+} indicating that Ti^{3+} has a key role in the photocatalytic performance of NiT nanocomposites.

Table S8. Product analysis of glycerol oxidation in **anaerobic** and **aerobic** conditions under direct sunlight obtained over NiT-3.

Product	Anaerobic condition			Aerobic condition		
	Yield (mmol/g.h)	Selectivity (%)[#]	Conversion (%)	Yield (mmol/g.h)	Selectivity (%)[#]	Conversion (%)
Glycolaldehyde	1.17	51.1	5	2.26	45.47	11
Formic Acid	0.32	13.97		0.65	13.08	
DHA	0.80	34.93		2.06	41.45	
CO_2	ND	ND		3.5	NA	
H_2	15.62	NA		0.92	NA	

#: Selectivity among the organic liquid products obtained by glycerol oxidation

Table S9: Product analysis of glycerol oxidation in **anaerobic** and **aerobic** condition under one sun condition obtained over NiT-3.

Product	Anaerobic condition			Aerobic condition		
	Yield (mmol/g.h)	Selectivity (%)[#]	Conversion (%)	Yield (mmol/g.h)	Selectivity (%)[#]	Conversion (%)
Glycolaldehyde	0.82	50.93	3.5	1.35	46.88	6
Formic Acid	0.23	14.29		0.55	19.1	
DHA	0.56	34.78		0.98	34.02	
CO_2	ND	ND		1.78	NA	
H_2	10.92	NA		0.65	NA	

#: Selectivity among the organic liquid products obtained by glycerol oxidation

Table S10. No. of electrons used for the production of H_2 and no. of holes used for glycerol oxidation to liquid products (Glycolaldehyde, DHA and Formic acid) with NiT-3 under direct sunlight in anaerobic and aerobic conditions.

Product	Anaerobic condition			Aerobic condition		
	Concentration (mmol/g.h)	No. of e^-/h^+ consumed (mmol/h.g)	e^-/h^+ ratio	Concentration (mmol/g.h)	No. of e^-/h^+ consumed (mmol/h.g)	e^-/h^+ ratio
Hydrogen	15.62	31.24	7.8	0.92	1.84	0.26
Glycolaldehyde	1.17	1.56		2.26	1.33	
DHA	0.80	1.60		2.06	4.12	
Formic acid	0.32	0.85		0.65	1.73	

Water to Hydrogen: $2\ H^+ + 2\ e^- \rightarrow H_2$ $n = 2$

Glycerol to Glycolaldehyde: $2\ C_3H_8O_3 \rightarrow 3\ C_2H_4O_2 + 4H^+ + 4e^-$ $n = \frac{4}{3}$

Glycerol to DHA: $C_3H_8O_3 \rightarrow C_3H_6O_3 + 2H^+ + 2e^-$ $n = 2$

Glycerol to Formic acid: $C_3H_8O_3 \rightarrow 3\ CH_2O_2 + 8H^+ + 8e^-$ $n = \frac{8}{3}$

where n means number of h^+ or e^- to transform glycerol or water into a specific product.[3]

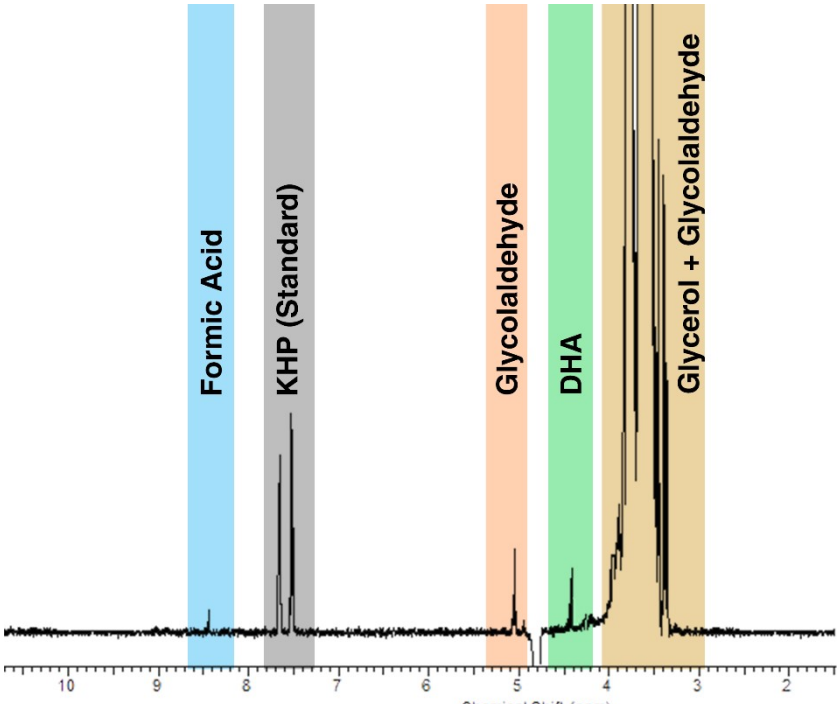

Figure S12.[1]H NMR spectra of the glycerol oxidation (water suppression sequence was performed): Using NiT-3 photocatalyst in anaerobic condition under direct sunlight.

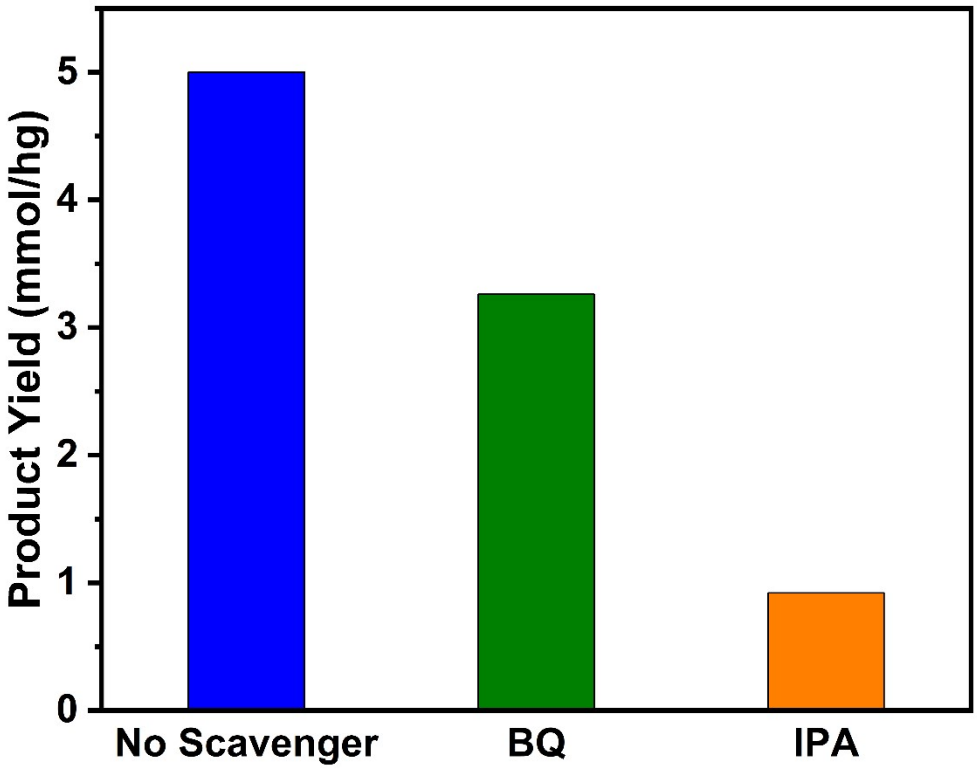

Figure S13. Influence of addition of scavengers, p-benzoquinone (BQ) and isopropanol (IPA) in the rate of photocatalytic oxidation of aqueous glycerol with NiT-3 nanocomposite in thin film form.

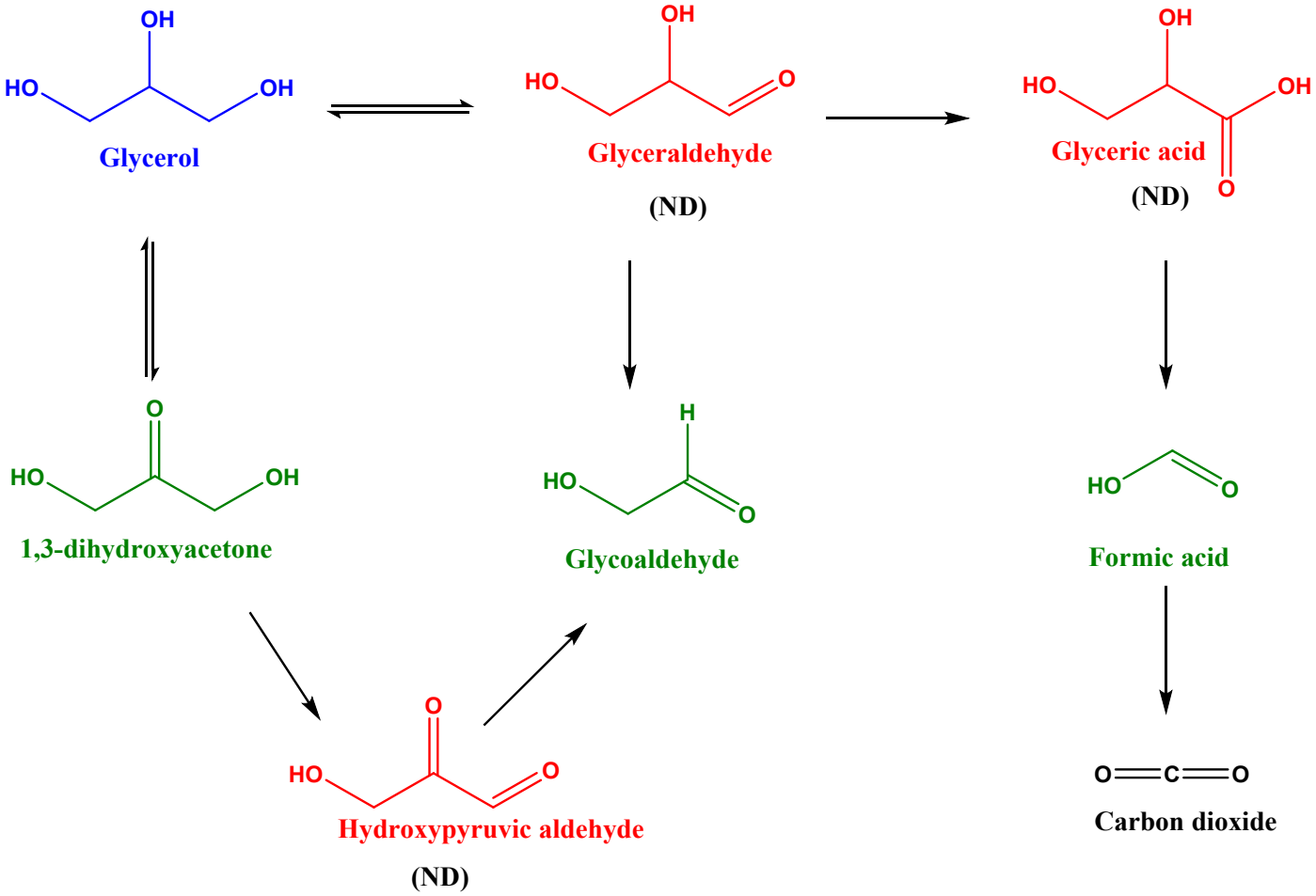

ND: Not Detected

Figure S14: Plausible reaction pathway for glycerol oxidation to value added products over NiT nanocomposites. Experimentally detected/measured products are shown in green and those compounds not observed is given in red.

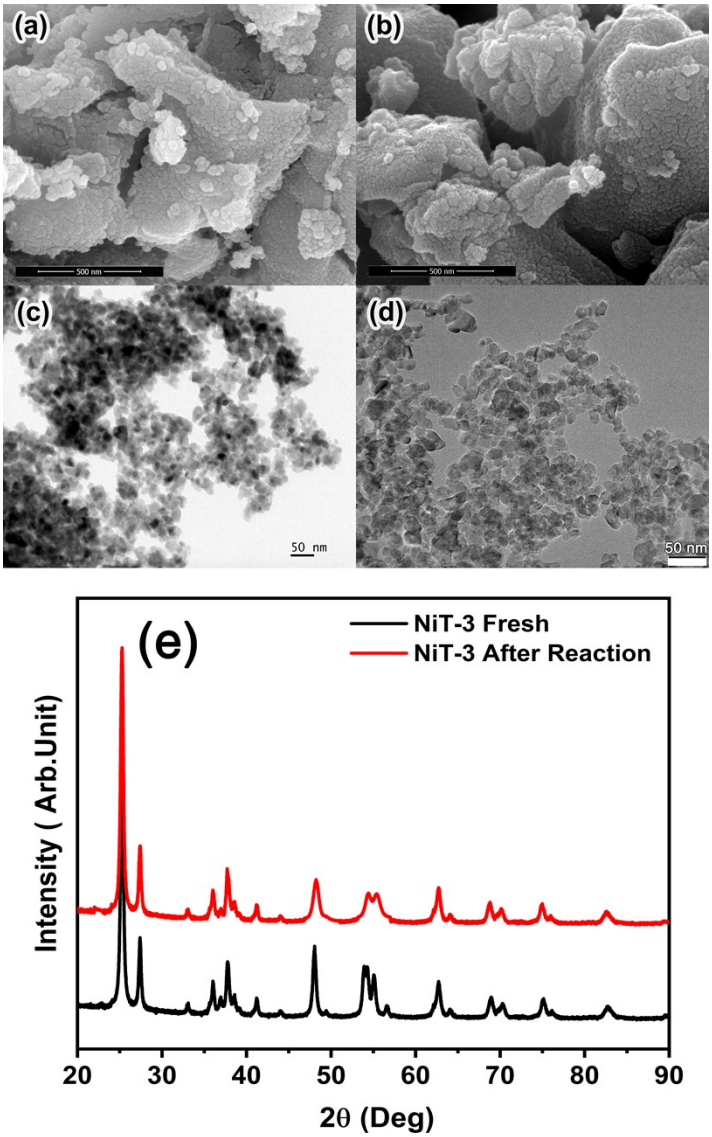

Figure S15. FESEM image of NiT-3 before (a) and after (b) recycling. TEM image of NiT-3 before (c) and after (d) recycling, and (e) comparison of PXRD patterns of fresh and spent NiT-3 sample.

Table S11. A summary of the H_2 yield reported from previous literature over various NiO species incorporated TiO_2 based photocatalysts in glycerol- water solution is compared with present work.

Photocatalyst	Light source	H_2 Yield ($mmolh^{-1}g^{-1}$)	Other products obtained	Reference
NiO/TiO_2	200 W Hg-Xe lamp	0.048	CO_2	[4]
$NiO\text{-}TiO_2$	300 W Xenon lamp	8	Glyceraldehyde and dihydroxyacetone	[5]
NiO_x/TiO_2	500 W high-pressure Hg lamp	0.9	CO, CO_2 and CH_4	[6]
NiO/TiO_2	500 W high-pressure Hg lamp	1.23	CO, CO_2 and CH_4	[7]
$NiO/Ti^{3+}\text{-}TiO_2$ nanocomposites	Sunlight	15.62	Dihydroxyacetone, glycolaldehyde and formic acid	Present work

S1: Video for hydrogen generation from thin film form of NiT-3 in direct sunlight. Pl. see the video File in .mp4 format.

Reference

1 M. Chauhan, K. Soni, P. E. Karthik, K. P. Reddy, C. S. Gopinath and S. Deka, *J. Mater. Chem. A*, 2019, **7**, 6985–6994.

2 B. Antil, L. Kumar, R. Ranjan, S. Shenoy, K. Tarafder, C. S. Gopinath and S. Deka, *ACS Appl. Energy Mater.*, 2021, **4**, 3118–3129.

3 Y.-H. Wu, D. A. Kuznetsov, N. C. Pflug, A. Fedorov and C. R. Müller, *J. Mater. Chem. A*, 2021, **9**, 6252.

4 S. P. Ramírez, J. A. Wang, M. A. Valenzuela, L. F. Chen and A. Dalai, *J. Appl. Res. Technol.*, 2020, **18**, 390–409.

5 M. Eisapour, H. Zhao, J. Zhao, T. Roostaei, Z. Li, A. Omidkar, J. Hu and Z. Chen, *J. Colloid Interface Sci.*, 2023, **647**, 255–263.

6 R. Liu, H. Yoshida, S. ichiro Fujita and M. Arai, *Appl. Catal. B Environ.*, 2014, **144**, 41–45.

7 S. ichiro Fujita, H. Kawamori, D. Honda, H. Yoshida and M. Arai, *Appl. Catal. B Environ.*, 2016, **181**, 818–824.